Inorg. Chem. **2009**, *48*, 4331−4341

1,4-Phenylenebis(methylidyne)tetrakis(phosphonic acid): A New Building Block in Metal Organic Framework Synthesis

Monika Plabst and Thomas Bein*

Department of Chemistry and Biochemistry, University of Munich, Butenandtstr. 5-13(E), D-81377 Munich, Germany

Received November 30, 2008

Through the use of a synthetic high-throughput approach, 1,4-phenylenebis(methylidyne)-tetrakis(phosphonic acid), **H_8L**, was investigated as a molecular building block for the formation of coordination frameworks with lanthanides (Ln = La, Nd, Gd, Dy) under hydrothermal conditions. Thereby, 14 new lanthanide phosphonates were discovered, categorized into three structure types, and their crystallization fields described. Structure type **I** comprises six compounds with the general formula **$Ln(H_5L)$**. The examples of $Ln[(PO_3H)_2CH-C_6H_4-CH(PO_3H)(PO_3H_2)]\cdot 4H_2O$, where Ln = La, and Nd, reveal two-dimensional coordination networks having a layered structure but differ in the layer stacking. Structure type **II** comprises four compounds of the general formula **$Ln_2(H_2L)$** and is represented by $La_2[(HO_3P)(O_3P)CH-C_6H_4-CH(PO_3)(PO_3H)]\cdot 8H_2O$, a layered structure with dimeric lanthanum coordination polyhedra. Four compounds of the type **$NaLn(H_4L)$** are in stucture type **III**, which was solved from $LaNa[(PO_3H)_2CH-C_6H_4-CH(PO_3H)_2]\cdot 4H_2O$. This structure consists of a three-dimensional open framework with La^{3+} coordinated by bisphosphonate units in an exclusively bidentate fashion. It has a one-dimensional rhombic channel system that is occupied by sodium ions and water molecules acting as guests.

Introduction

Metal organic frameworks (MOFs) have raised considerable interest in both academia and industry due to their fascinating structural chemistry and their potential applications in the field of gas separation and storage, as well as catalysis and chemical sensing. They are composed of organic linkers and metal complexes or clusters, both units acting as building blocks that are often intended to assemble into a three-dimensional open framework. The majority of MOF structures rely on carboxylate derivatives as bidentate ligands having a regular coordination mode with d-block metal ions.[1,2] Conceptually, this leads to the secondary building unit approach.[3,4] In contrast, in organometalphosphonate chemistry, control over the formation of geometrically well-defined structures has not been obtained yet due to the highly variable coordination modes of the phosphonate group. It can act as mono- or bidentate ligand for one, or in combination for various metal centers. In most cases, this flexibility allows the metal phosphonate groups to pack efficiently in inorganic layers. This explains the propensity of phosphonate ligands toward layered or pillared solids.[5−13] In fact, the first phosphonates with significant porosity were obtained in the form of pillared solids.[14,15] However, these materials tend to feature low crystallinity, and details of their structure are difficult to obtain. Only few crystalline phosphonate-based three-dimensional coordination

* To whom correspondence should be addressed. E-mail: bein@lmu.de.

(1) Cheetham, A. K.; Feller, R. K. *Chem.Commun.* **2006**, 4780–4795.
(2) Rosseinsky, M. J. *Microporous Mesoporous Mater.* **2004**, *73*, 15–30.
(3) Eddaoudi, M.; Moler, D. B.; Li, H.; Chen, B.; Reineke, T. M.; O'Keeffe, M.; Yaghi, O. M. *Acc. Chem. Res.* **2001**, *34*, 319–330.
(4) Tranchemontagne, D. J.; Ni, Z.; O'Keeffe, M.; Yaghi, O. M. *Angew. Chem., Int. Ed.* **2008**, *47*, 5136–5147.
(5) Clearfield, A., *Metal Phosphonate Chemistry*; John Wiley & Sons, Inc.: New York, 1998; Vol. *47*, p 992.
(6) Rabu, P.; Janvier, P.; Bujoli, B. *J. Mater. Chem.* **1999**, *9*, 1323–1326.
(7) Stock, N.; Bein, T. *J. Solid State Chem.* **2002**, *167*, 330–336.
(8) Irran, E.; Bein, T.; Stock, N. *J. Solid State Chem.* **2003**, *173*, 293–298.
(9) Gomez-Alcantara, M. d. M.; Cabeza, A.; Moreno-Real, L.; Aranda, M. A. G.; Clearfield, A. *Microporous Mesoporous Mater.* **2006**, *88*, 293–303.
(10) Konar, S.; Zon, J.; Prosvirin, A. V.; Dunbar, K. R.; Clearfield, A. *Inorg. Chem.* **2007**, *46*, 5229–5236.
(11) Cabeza, A.; Aranda, M. A. G.; Bruque, S.; Poojary, D. M.; Clearfield, A.; Sanz, J. *Inorg. Chem.* **1998**, *37*, 4168–4178.
(12) Serpaggi, F.; Ferey, G. *J. Mater. Chem.* **1998**, *8*, 2749–2755.
(13) Stock, N.; Guillou, N.; Bein, T.; Ferey, G. *Solid State Sci.* **2003**, *5*, 629–634.
(14) Clearfield, A. *Dalton Trans.* **2008**, 6089–6102.
(15) Wang, Z.; Heising, J. M.; Clearfield, A. *J. Am. Chem. Soc.* **2003**, *125*, 10375–10383.

10.1021/ic802294e CCC: $40.75
Published on Web 04/14/2009

polymers with open frameworks have been[16,17]described up to now. When searching for three-dimensional inorganic−organic hybrid networks, the phosphonate functionality is often used in combination with other functional groups such as carboxylates, sulfonates, or pyridinium groups.[10,18−25] Similar to the challenges found in phosphonate structural chemistry, a lack of control is often observed in synthesis approaches using lanthanides as metal centers for coordination polymers.[26] Their fluorescence[27−35] and magnetic[28,36] properties make lanthanides highly attractive for the synthesis of functional materials. However, in the absence of design strategies, it is difficult to target materials with specific structures and, hence, properties. With their high and flexible coordination numbers, lanthanides extend the number of coordination geometries covered by transition metals, which are typically used in MOF synthesis. On the other hand, due to the high coordination numbers, lanthanide coordination geometries are difficult to control with common small MOF ligands such as carboxylates[37−41] or even monophosphonates.[42]

Scheme 1

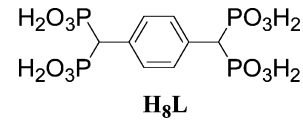

H_8L

In order to address these issues, we have explored the potential of the new ligand 1,4-phenylenbis(methylidyne)-tetrakis (phosphonic acid), **H_8L**, as a new building block in the phosphonate family (Scheme 1). Featuring two bisphosphonate groups as bidentate chelating ligands, **H_8L** is able to complex large ions with high coordination numbers, such as lanthanides, with a well-defined geometry that is common for carboxylate ligands and small ions such as zinc or copper.[43] Through the use of a synthetic high-throughput approach, **H_8L** was screened in combination with different lanthanides and under different synthesis conditions. For this purpose, we have developed a multiclave system permitting the investigation of up to 24 hydrothermal syntheses at once. The methodology includes automated dosing of liquids, subsequent parallel synthesis, isolation, and automatic characterization by X-ray diffraction.[44]

Experimental Section

Bisphosphonic Acid Synthesis. Solvents and chemicals were purchased from Aldrich, Fluka, and Merck and were used as received. Organic reactions were carried out under inert gas, and glassware was heated before use. Products were dried under high vacuum conditions. Thin-layer chromatography (TLC) and flash column chromatography were performed on silica TLC plates (Merck, Kieselgel60 F254 Merck) and Silicagel 60 (grain size 0.040−0.063 mm), respectively. Elution was performed under pressure. IR spectra were recorded on a Bruker IFS 28 Equinox 55 spectrometer. Liquid samples were measured as films between two KBr plates. Band locations are indicated as wavenumbers in centimeters^{-1}. NMR spectra were recorded at room temperature on a JEOL EX 400 and a JEOL GSX 270. The chemical shift is given relative to tetramethylsilane. The solvent signal was used as an internal standard. Peaks were assigned with the help of correlation spectroscopy, heteronuclear multiple-bond correlation, and heteronuclear single quantum coherence spectra. Mass spectrometry was carried out on a Finnigan MAT 95Q. Electron bombardment ionization was carried out at a source temperature of 250 °C and with an electron energy of 70 eV. For direct exposure probe mass spectroscopy, samples were heated on a platinum wire from 20 to 1600 °C with a heating rate of 120 °C/min. Elemental analysis was performed on an ELEMENTAR vario EL.

Tetraethyl-[1,4-phenylenbis(methylen)]-bisphosphonate, 1. *p*-Dibromoxylene (15.40 mmol, 4.07 g) was dissolved in toluene (100 mL) by slight heating. Then, triethyl phosphite was added, and the resulting mixture was stirred at 111 °C under a nitrogen flow. The reaction was monitored by TLC. After 20 h, the mixture was cooled down to room temperature, and the solvent was evaporated in vacuo. The resulting solid was purified by flash column chromatography, eluting with ethyl acetate/methanol (85:15) to yield **1** (5.41 g, 14.30 mmol, 93%) as a white solid. IR (KBr): ν_{max} = 2983, 2952, 2911, 2909, 1514, 1480, 1439, 1430 (sh), 1392, 1367, 1300 (sh), 1242, 1201, 1161, 1140, 1011, 1088, 1033, 961, 864, 833 (sh), 822, 801,

(16) Kong, D.; McBee, J.; Clearfield, A. *Inorg. Chem.* **2006**, *45*, 977–986.
(17) Liang, J.; Shimizu, G. K. H. *Inorg. Chem.* **2007**, *46*, 10449–10451.
(18) Cao, D.-K.; Li, Y.-Z.; Song, Y.; Zheng, L.-M. *Inorg. Chem.* **2005**, *44*, 3599–3604.
(19) Cao, D.-K.; Liu, Y.-J.; Song, Y.; Zheng, L.-M. *New J. Chem.* **2005**, *29*, 721–725.
(20) Bauer, S.; Bein, T.; Stock, N. *J. Solid State Chem.* **2006**, *179*, 145–155.
(21) Cao, D.-K.; Xiao, J.; Li, Y.-Z.; Clemente-Juan, J. M.; Coronado, E.; Zheng, L.-M. *Eur. J. Inorg. Chem.* **2006**, 1830–1837.
(22) Bauer, S.; Stock, N. *J. Solid State Chem.* **2007**, *180*, 3111–3120.
(23) Cao, D.-K.; Li, Y.-Z.; Zheng, L.-M. *J. Solid State Chem.* **2006**, *179*, 573–578.
(24) Sonnauer, A.; Naether, C.; Hoeppe, H. A.; Senker, J.; Stock, N. *Inorg. Chem.* **2007**, *46*, 9968–9974.
(25) Bauer, S.; Marrot, J.; Devic, T.; Ferey, G.; Stock, N. *Inorg. Chem.* **2007**, *46*, 9998–10002.
(26) Hill, R. J.; Long, D.-L.; Hubberstey, P.; Schroeder, M.; Champness, N. R. *J. Solid State Chem.* **2005**, *178*, 2414–2419.
(27) Glover, P. B.; Bassett, A. P.; Nockemann, P.; Kariuki, B. M.; Van Deun, R.; Pikramenou, Z. *Chem. Eur. J.* **2007**, *13*, 6286.
(28) Harbuzaru, B. V.; Corma, A.; Rey, F.; Atienzar, P.; Jorda, J. L.; Garcia, H.; Ananias, D.; Carlos, L. D.; Rocha, J. *Angew. Chem., Int. Ed.* **2008**, *47*, 1080–1083.
(29) Park, O.-H.; Seo, S.-Y.; Bae, B.-S.; Shin, J. H. *Appl. Phys. Lett.* **2003**, *82*, 2787–2789.
(30) Romanelli, M.; Kumar, G. A.; Emge, T. J.; Riman, R. E.; Brennan, J. G. *Angew. Chem., Int. Ed.* **2008**, *47*, 6049–6051.
(31) Sun, L.-N.; Zhang, H.-J.; Fu, L.-S.; Liu, F.-Y.; Meng, Q.-G.; Peng, C.-Y.; Yu, J.-B. *Adv. Funct. Mater.* **2005**, *15*, 1041–1048.
(32) Tang, Z.-H.; Liu, D.-Y.; Tang, Y.; Cao, X.-P. *Z. Anorg. Allg. Chem.* **2008**, *634*, 392–396.
(33) Yanagida, S.; Hasegawa, Y.; Murakoshi, K.; Wada, Y.; Nakashima, N.; Yamanaka, T. *Coord. Chem. Rev.* **1998**, *171*, 461–480.
(34) Yang, J.; Zhang, C.; Li, C.; Yu, Y.; Lin, J. *Inorg. Chem.* **2008**, *47*, 7262–7270.
(35) Zhong, J.; Liang, H.; Lin, H.; Han, B.; Su, Q.; Zhang, G. *J. Mater. Chem.* **2007**, *17*, 4679–4684.
(36) Lin, P.-H.; Burchell Tara, J.; Clerac, R.; Murugesu, M. *Angew. Chem., Int. Ed. Engl.* **2008**, *47*, 8848–51.
(37) Qiu, Y.; Liu, H.; Ling, Y.; Deng, H.; Zeng, R.; Zhou, G.; Zeller, M. *Inorg. Chem. Commun.* **2007**, *10*, 1399–1403.
(38) Zhao, J.; Long, L.-S.; Huang, R.-B.; Zheng, L.-S. *Dalton Trans.* **2008**, 4714–4716.
(39) Guo, X.; Zhu, G.; Li, Z.; Chen, Y.; Li, X.; Qiu, S. *Inorg. Chem.* **2006**, *45*, 4065–4070.
(40) Guo, X.; Zhu, G.; Sun, F.; Li, Z.; Zhao, X.; Li, X.; Wang, H.; Qiu, S. *Inorg. Chem.* **2006**, *45*, 2581–2587.
(41) Li, Z.; Zhu, G.; Guo, X.; Zhao, X.; Jin, Z.; Qiu, S. *Inorg. Chem.* **2007**, *46*, 5174–5178.
(42) Clearfield, A. *Chem. Mater.* **1992**, *4*, 864–871.
(43) Platt, A. W. G. *Inorg. Chim. Acta* **1994**, *223*, 43–53.
(44) Stock, N.; Bein, T. *Angew. Chem., Int. Ed.* **2004**, *43*, 749–752.

745, 709, 571, 500, 515, 485, 466, 449, 430. ^{31}P NMR (161.83 MHz, $CDCl_3$): δ 26.91 ($^2J_{HP}$ = 7.8). ^{1}H NMR (400 MHz, $CDCl_3$): δ 1.22, 12H, t ($^1J_{HH}$ = 7.0), 4 × $CH_2C\mathbf{H_3}$; 3.11, 4H, d ($^2J_{HP}$ = 20.2), 2 × CHP; 3.99, 8H, m, 4 × OCH_2; 7.23, 4H, s, CH_{ar}. ^{13}C NMR (100.53 MHz, $CDCl_3$): δ 16.45, 4 × CH_3, t ($^3J_{CP}$ = 3.14), CH_3; 33.00, 2 × CH, d ($^1J_{CP}$ = 139.2), CP; 62.17, 4 × CH_2, t ($^2J_{CP}$ = 3.16), OCH_2; 130.00, 4 × CH, C_{ar}; 130.33, 2 × C_q, C_{ipso}. HRMS (GC/EI) calcd for $C_{16}H_{28}O_6P_2$: 378.1361 gmol^{-1} [M^+]. Found: 378.1353.

Octaethyl-[1,4-phenylenebis(methylidyne)tetrakisphosphonate], 2. To a solution of **1** (5 g, 13.2 mmol) in 150 mL of anhydrous THF at −78 °C was added 4 equiv of lithium diisopropylamide (30.1 mL of a 1.8 M solution). After 5 min of stirring, diethyl chlorophosphate (4.79 g, 27.78 mmol) was added, and the reaction mixture turned green for a moment. The mixture was slowly warmed to room temperature and stirred. After 2 h, the reaction was quenched by the addition of a saturated NH_4Cl solution and the solvent evaporated in vacuo. The yellow residue was refluxed in diethyl ether to remove undesired byproducts and then separated from the organic layer by filtration, dissolved in 200 mL of CH_2Cl_2, washed with water and a saturated NaCl solution, and dried over anhydrous Na_2SO_4, and the solvent was evaporated in vacuo to yield **2** (3.83 g, 5.9 mmoL 49%) as a white powder. IR (KBr): ν_{max} = 2987, 2932, 2913, 2878, 1511, 1442, 1430 (sh), 1393, 1368, 1304 (sh), 1252, 1239, 1223 (sh), 1179 (sh), 1162, 1098, 1053, 1020, 981 (sh), 965, 949 (sh), 895, 860, 808, 791, 750, 694, 582 (sh), 563, 497, 486, 458, 444(sh), 415. ^{31}P NMR (161 MHz, $CDCl_3$): δ 18.81 ($^2J_{HP}$ = 23,5 Hz). ^{1}H NMR (400 MHz, $CDCl_3$): δ 1.06, 12H, m, 8 × $CH_2C\mathbf{H_3}$; 1.18, 12H, m, 8 × $CH_2C\mathbf{H_3}$; 3.64, 2H, t ($^2J_{HP}$ = 24.6), 2 × CHP_2; 3.88, 4H, m, 4 × $OC\mathbf{H_A}H$; 3.98, 4H, m, 4 × $OC\mathbf{H_B}H$; 4.03, 8H, m, 4 × $OC\mathbf{H_2}$; 7.38, 4H, s, CH_{ar}. ^{13}C NMR (100.53 MHz, $CDCl_3$): δ 16.21, 4 × CH_3, m, $CH_2C\mathbf{H_3}$; 16.32, 4 × CH_3, m, $CH_2C\mathbf{H_3}$; 45.37, 2 × CH, t ($^1J_{CP}$ = 133.0), CHP_2; 62.92, 4 × CH_2, OCH_2; 63.37, 4 × CH_2, OCH_2; 129.83, 2 × C_q, C_{ipso}; 130.62, 4 × CH; C_{ar}. HRMS (GC/EI) calcd for $C_{24}H_{46}O_{12}P_4$: 650.1940 [M^+]. Found: 650.1918.

1,4-Phenylenebis(methylidyne)tetrakis(phosphonic acid), H_8L. To a solution of **2** (2.85 g, 4.39 mmol) in 20 mL of dry CH_2Cl_2 was added trimethylsilybromide (5.34 g, 39.50 mmol), and the reaction mixture was stirred under a nitrogen flow. The reaction was monitored by TLC. After 4 h, the reaction was quenched with 50 mL of MeOH and the solvent evaporated. The residue was recrystallized from diethylether and methanol to obtain **H_8L** as a white powder (4.39 mmol, >99%) that reacts acidic in aqueous solution. IR (KBr): ν_{max} = 2901, 2842, 2278, 1924, 1632, 1506, 1460, 1429, 1306, 1241, 1202, 1156, 1136 (sh), 1031, 1022 (sh), 972 (sh), 962 (sh), 937, 845, 797, 770, 714, 562, 509, 479, 435, 410. ^{31}P NMR (MHz, D_2O): δ 17.84 ($^2J_{HP}$ = 24.3 Hz). ^{1}H NMR (400 MHz, D_2O): δ 3.78, 2H, t ($^2J_{HP}$ = 24.39 Hz), CHP_2; 7.24, 4H, s, CH_{ar}. ^{13}C NMR (100.53 MHz, D_2O): 46.67, 2 × CH, t ($^1J_{CP}$ = 126.10 Hz), CHP_2; 130.60, 4 × CH, C_{ar}; 131.58, 2 × C_q, C_{ipso}. Anal. calcd for $C_8H_{14}O_{12}P_4 \cdot 1.5H_2O$: C, 21.21; H, 3.78. Found: C, 21.37; H, 3.70.

Metalphosphonate Synthesis. The high-throughput screening experiments with **H_8L** were performed in custom-made multiclaves with 24 cavities containing individual Teflon liners of an individual total volume of 3 mL. Before each synthesis, the liners were cleaned in concentrated HCl and rinsed with water. They were deposited on a multistirrer device and equipped with small magnetic stirring bars. In order to facilitate the dosing, solutions were prepared from all reagents: In a volumetric flask, 25 mL of a 0.5 M solution of **H_8L** was prepared by dissolving 5.663 g of the ligand in deionized water. One molar solutions of lanthanide salts were prepared for $La(NO_3)_3 \cdot 6H_2O$, $Nd(NO_3)_3 \cdot 6H_2O$, $Gd(NO_3)_3 \cdot 6H_2O$, and $Dy(NO_3)_3 \cdot 6H_2O$ in deionized water. A 1 M NaOH standard solution was purchased from Aldrich. Reaction gels were prepared according to the following general procedure: The ligand solution was filled into the Teflon liner. Deionized water was added, and stirring was started. If applicable, NaOH was added. After subsequent addition of the metal-salt solution, precipitation occurred. The reaction mixture was stirred for 30 min until a homogeneous gel was formed. After the removal of the stirring bars, the pH was measured, and the Teflon liners were transferred to the reactor block, closed, and mounted into the multiclave. Subsequently, they were heated for 7 days at 75, 100, 150, or 180 °C, respectively. After the heating procedure, the pH was measured again, and crystals were separated from the reaction mixture by filtration under reduced pressure with the help of a custom-made multifrit and washed with water. The products were dried at room temperature, and XRDs were recorded. The discovery library was prepared from reactions with the following batch compositions:

Table 1. Optimal Synthesis Conditions for the New Lanthanide-Phosphonates and Single Crystals if Available

compound	batch composition	T/°C
$La(H_5L)$ a	$La(NO_3)_3/H_8L$/830 H_2O	150
$La(H_5L)$ c	$La(NO_3)_3/H_8L$/830 H_2O	180
$NaLa(H_4L)$	$La(NO_3)_3/H_8L$/4 NaOH/830 H_2O	100
$NaLa(H_4L)$, single crystal	$La(NO_3)_3/H_8L$/4 NaOH/8300 H_2O	100
$La_2(H_2L)$	4 $La(NO_3)_3/H_8L$/4 NaOH/830 H_2O	100
$La_2(H_2L)$, single crystal	6 $La(NO_3)_3/H_8L$/830 H_2O	100
$La(H_5L)$ b, single crystal	$La(NO_3)_3/H_8L$/8300 H_2O	150
$Nd(H_5L)$ d	$Nd(NO_3)_3/H_8L$/830 H_2O	150
$NaNd(H_4L)$	$Nd(NO_3)_3/H_8L$/4 NaOH/830 H_2O	150
$Nd_2(H_2L)$	6 $Nd(NO_3)_3/H_8L$/830 H_2O	100
$Nd(H_5L)$ b	$Nd(NO_3)_3/H_8L$/830 H_2O	180
$Nd(H_5L)$ a, single crystal	$Nd(NO_3)_3/H_8L$/4 NH_3/16660 H_2O	150
$Gd(H_5L)$ d	$Gd(NO_3)_3/H_8L$/830 H_2O	75
$NaGd(H_4L)$	$Gd(NO_3)_3/H_8L$/4 NaOH/830 H_2O	100
$Gd_2(H_2L)$	2 $Gd(NO_3)_3/H_8L$/4 NaOH/830 H_2O	100
$Dy(H_5)$L e	$Dy(NO_3)_3/H_8L$/830 H_2O	100
$NaDy(H_4L)$	$Dy(NO_3)_3/H_8L$/4 NaOH/830 H_2O	150
$Dy_2(H_2L)$	6 $Dy(NO_3)_3/H_8L$/4 NaOH/830 H_2O	75

$$x\text{La}(NO_3)_3/H_8L/y\text{NaOH}/830\ H_2O$$
$$x\text{Nd}(NO_3)_3/H_8L/y\text{NaOH}/830\ H_2O \quad x = 1, 2, 4, \text{and } 6$$
$$x\text{Dy}(NO_3)_3/H_8L/y\text{NaOH}/830\ H_2O \quad y = 0, 4, \text{and } 8$$
$$x\text{Gd}(NO_3)_3/H_8L/y\text{NaOH}/830\ H_2O$$

A typical batch volume was 1.5 mL. In order to obtain crystals suitable for single-crystal structure analysis, dilution series of all new compounds were generated under the conditions that provided best crystallinity according to XRD, or that showed large crystals in the optical microscope. For this purpose, the synthesis time, temperature, and composition of the respective batches were maintained, except for the water content z:

$$x\text{Ln}(NO_3)_3/H_8L/y\text{NaOH}/zH_2O$$
$$z = 830, 1660, 2075, 8300, 16600, 83000$$

The highest dilution degree at z = 83 000 corresponds, in a typical batch with a 1.5 mL volume, to a total amount of reactants of about 1 mg. This was the lowest amount that could be accurately dosed. The best crystallization conditions for each new phase and the conditions that allowed the growth of single crystals are listed in Table 1. A detailed description of the respective syntheses including the information about yield and energy dispersive X-ray (EDX) characterization is given in the Supporting Information, section 1.

Scheme 2

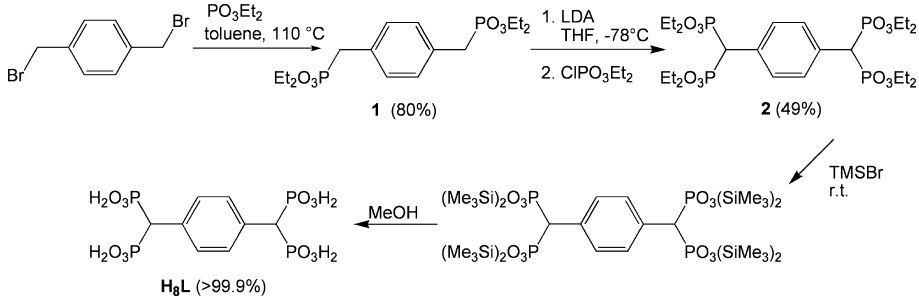

Metalphosphonate Characterization. A high-throughput X-ray analysis of all samples of the discovery library was carried out using a Stoe high-throughput powder diffractometer equipped with an image plate detector system.[44] Higher-resolution X-ray powder diffraction patterns were recorded from all new phases in $\theta-\theta$ geometry with a Bruker D8 Discover instrument using monochromatic Cu K_α radiation and a Vantec detector. Morphology and stoichiometry were studied with a Jeol JSM 6500 F scanning electron microscope equipped with an EDX detector. The respective samples were applied to an adhesive carbon film on the sample holder and coated with carbon by a BAL-TEC MED 020 Coating System. Raman spectra were recorded on a Jobin Yvon Horiba HR800 UV Raman microscope using a HeNe laser emitting at 632.8 nm. Thermogravimetric analyses (TGA) were performed on a Netzsch STA 449 C TG/DSC (heating rate of 10 K/min in a stream of synthetic air of ~25 mL/ min). The chemical compositions of representatives of each new structure type were determined by inductively coupled plasma optical emission spectroscopy (ICP-OES, VARIAN VISTA) and an ELEMENTAR vario EL.

Crystallography. Cell determination and data collection for single-crystal structure analysis by X-ray diffraction were performed on an Enraf-Nonius Kappa-CCD diffractometer equipped with a rotating anode (Mo K_α radiation, $\lambda = 71.073$ pm). All single-crystal structures were solved by direct methods and refined using the program package SHELXTL.[45]

Nd(H_5L) a. A structure analysis of the rods revealed the composition $Nd[(PO_3H)_2CH-C_6H_4-CH(PO_3H)(PO_3H_2)]\cdot 4H_2O$. The structure was solved with direct methods in the triclinic space group $P\bar{1}$. All hydrogen atoms except those from water could be localized in the difference Fourier map. Crystallographic data are listed in Table S7a,[46] selected bond distances in Table S7b−d.

La(H_5L) b. A structure analysis of the colorless rods revealed the composition $La[(PO_3H)_2CH-C_6H_4-CH(PO_3H)(PO_3H_2)]\cdot 4H_2O$. Structure solution succeeded in the triclinic space group $P\bar{1}$. All hydrogen atoms could be localized in the difference Fourier map. The positions of the hydrogen atoms next to O2 and O12 are only half-occupied. Crystallographic data are listed in Table S7a; selected bond distances are listed in the Table S7e−g.

La_2(H_2L). A structure analysis of the colorless blocks revealed the composition $La_2[(HO_3P)(O_3P)CH-C_6H_4-CH(PO_3)(PO_3H)]\cdot 8H_2O$. Structure solution succeeded in the triclinic space group $P\bar{1}$. All hydrogen atoms could be localized in the difference Fourier map. Crystallographic data are listed in Table S7a; selected bond distances are listed in the Table S7h−j.

NaLa(H_4L). A structure analysis of the rhombic crystals revealed the composition $LaNa[(PO_3H)_2CH-C_6H_4-CH(PO_3H)_2]\cdot 4H_2O$. The structure was solved with direct methods in the monoclinic space group $P2_1/n$. All hydrogen atoms with the exception of the water-hydrogen bonded to O15 could be localized in the difference Fourier map. Crystallographic data are listed in Table S7a; selected bond distances are listed in Table S7k−m.

Results and Discussion

H_8L was prepared in four steps starting from xylylene dibromide (Scheme 2). The monophosphonate groups were introduced via an Arbusov reaction.[47] Treatment of xylylene-dibromide with triethyl phosphite provided tetraethyl-[1,4-phenylenbis(methylen)]-bisphosphonate, **1**, in 80% yield. The phosphonate was then converted to the corresponding lithium salt using 4 equiv of lithium diisopropylamide, and the subsequent reaction with diethyl chlorophosphate gave octaethyl-[1,4-phenylenebis(methylidyne) tetrakisphosphonate], **2**, in 49% yield.[48] The appearance of a triplet ^{13}C NMR signal at 45 ppm indicated that the second phosphonate group in the benzyl position was introduced successfully. Finally, hydrolysis of this compound was achieved at excellent overall yield by transesterification to the corresponding tetra(trimethylsilyl)ester, **3**, followed by the addition of methanol.[49]

In the *high-throughput screening*, the organic building block **H_8L** was reacted with La^{3+}, Nd^{3+}, Dy^{3+}, and Gd^{3+} ions under hydrothermal conditions. The metal-to-ligand ratios in the synthesis solutions were selected as 1:1, 2:1, 4:1, and 6:1, considering the possible formation of single-metal nodes and cluster nodes in three-dimensional open frameworks. The pH was adjusted with sodium hydroxide. The NaOH-to-ligand ratios were 0:1, 4:1, and 8:1, thus covering a pH range from pH = 1 to pH = 7−8. No reactions were carried out under alkaline conditions because of the expected precipitation of lanthanide hydroxides in basic media. Crystallization proceeded under hydrothermal conditions for 7 days at 75, 100, 150, or 180 °C. Thus, a discovery library of 96 samples was generated and evaluated by comparing the X-ray powder patterns of all products. Four important crystallization fields could be identified, represented here in a three-dimensional plot of the reaction parameters as green, blue, yellow, and red regions (Figure 1). Within the described parameter range, 14 new compounds were found, which could be assigned to three structure types with the general formulas **Ln(H_5L)**, **Ln_2(H_2L)**, and **NaLn(H_4L)** (Figure 2). The six compounds within structure

(45) Sheldrick, G. *Acta Crystallogr., Sect. A* **2008**, *64*, 112–122.
(46) Figures marked with S are shown in the Supporting Information.
(47) Quin, L. D., *A Guide To Organophosphorous Chemistry*, 1st ed.; John Wiley & Sons: New York, 2000; p 394.
(48) Arstad, E.; Hoff, P.; Skattebol, L.; Skretting, A.; Breistol, K. *J. Med. Chem.* **2003**, *46*, 3021–32.
(49) McKenna, C. E.; Higa, M. T.; Cheung, N. H.; McKenna, M. C. *Tetrahedron Lett.* **1977**, 155–8.

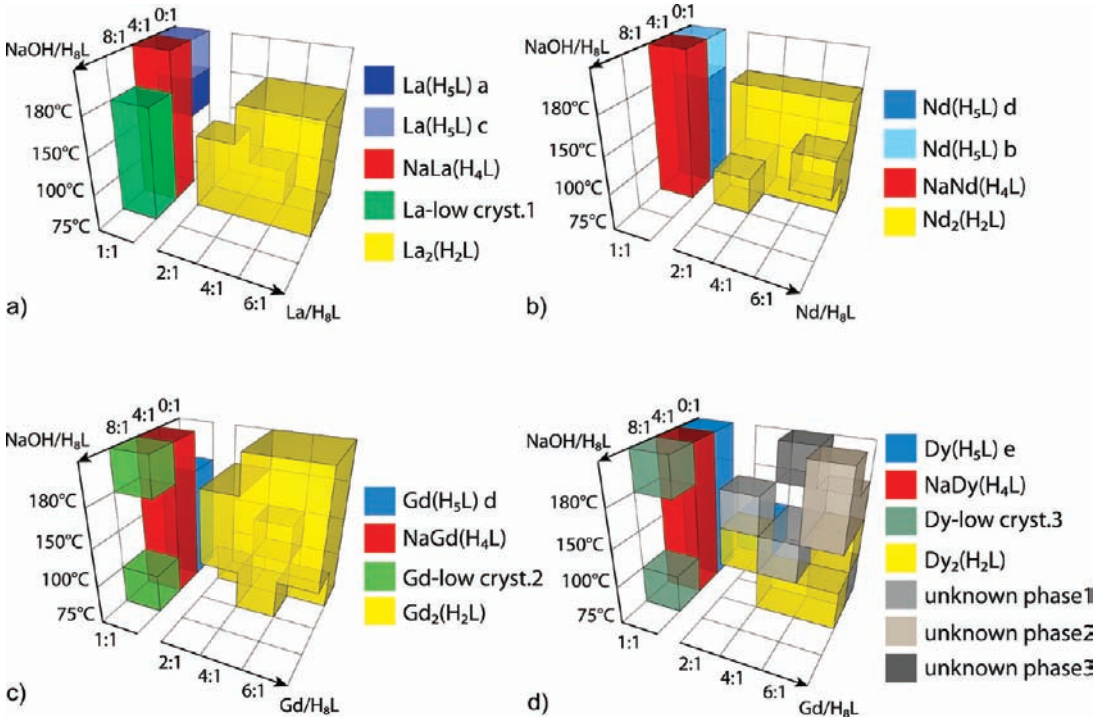

Figure 1. Results of the high-throughput screening of **H_8L** with La^{3+} (a), Nd^{3+} (b), Gd^{3+} (c), and Dy^{3+} (d). Only crystallographically pure phases are represented. An X-ray diffractogram of each phase is shown in the Supporting Information, section 2.

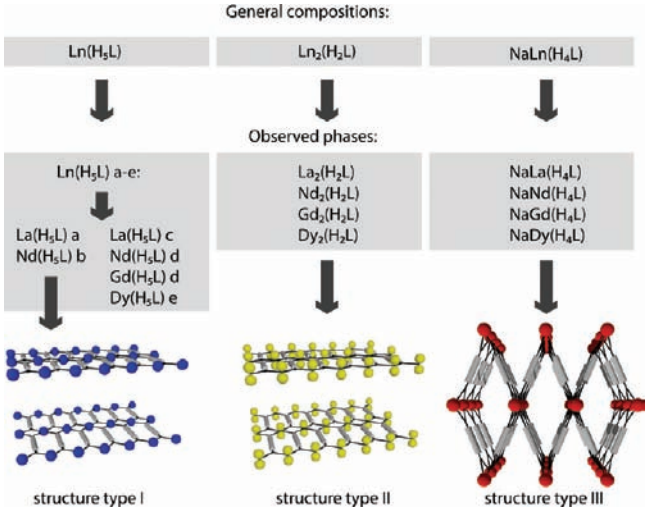

Figure 2. Assignment of the phases that crystallize in the blue-, yellow-, and red-coded regions of the parameter field, to three structure types. The subcategories (**a**−**e**) in structure type **I** stand for different layer stackings.

type **I** were further subclassified into **Ln(H$_5$L) a**−**e** due to their different layer stackings.

Generally, the parameter range for successful crystallization was limited by the pH. The reaction media were strongly acidic at NaOH-to-H_8L ratios of 0:1 and 4:1 and neutral to slightly basic at a NaOH-to-H_8L ratio of 8:1. Highly crystalline products were observed in the blue, yellow, and red regions, which are located in the parameter field with acidic conditions. In neutral to slightly basic media, crystallization was only observed at a metal-to-ligand ratio of 1:1 (Figure 1, green), where the poorly crystalline phases 1−3 were observed. They show powder patterns consisting of only a few broad signals (Figures S2d, S2l, S2p). Additionally, their morphology indicates the formation of poorly ordered layered materials.

More interesting are the blue regions, which represent layered compounds with the composition **Ln(H$_5$L)**. They were all formed at a lanthanide-to-ligand ratio of 1:1 without any NaOH addition. Slight changes in this crystallization system, such as variation of the lanthanide or the crystallization temperature, led to the formation of phases **Ln(H$_5$L) a**−**e** (Figure 2). Providing La^{3+} as a framework metal, **La(H$_5$L) a** crystallized at 150 °C and **La(H$_5$L) c** at 180 °C (Figure 1a). When $NdNO_3$ was the metal source, **Nd(H$_5$L) b** was formed in the temperature range from 75 to 150 °C and **Nd(H$_5$L) d** at 180 °C (Figure 1b). In the Gd^{3+}-containing system, **Gd(H$_5$L) d** crystallized in the range of 75−150 °C (Figure 1c). With Dy^{3+}, **Dy(H$_5$L) e** was formed over the whole temperature range (Figure 1d). A comparison of the powder patterns of these six compounds reveals the presence of five crystallographically different phases (**a**−**e**; Figure 3). **Nd(H$_5$L) d** and **Gd(H$_5$L) d** are isomorphous. The structures of **Ln(H$_5$L) a** and **Ln(H$_5$L) b** could be solved.

The fine needles of **La(H$_5$L) a** were not suitable for single-crystal structure analysis. However, performing a synthetic dilution series, the same structure type could be obtained with Nd^{3+} as a lattice metal under more dilute conditions and in the presence of small amounts of ammonia (**Nd(H$_5$L) a**). **Nd(H$_5$L) a** was obtained in the form of single crystals. The powder pattern simulated from the data of the structure solution of **Nd(H$_5$L) a** corresponds well with the experimental powder pattern of **La(H$_5$L) a** (Figure S2a). Therefore, the structure of **Nd(H$_5$L) a** (Figure 4) will be discussed as a representative for **Ln(H$_5$L) a** (Figure 2).

The asymmetric unit of **Nd(H$_5$L) a** contains 29 non-hydrogen atoms and 19 hydrogen atoms (Figure 4a). The

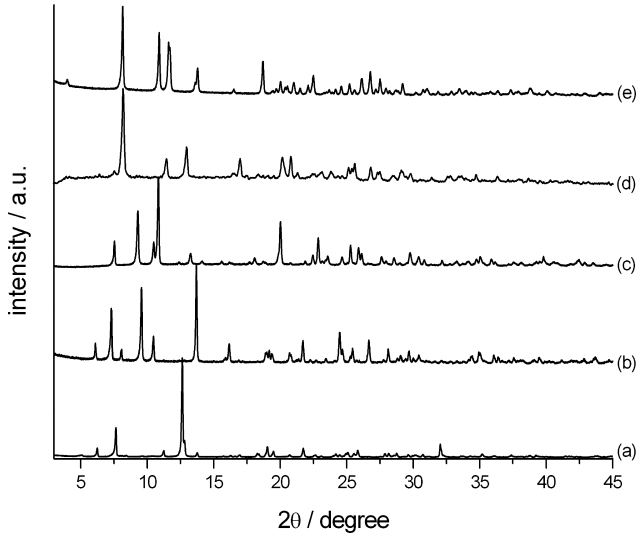

Figure 3. Powder patterns of phases crystallized at a lanthanide-to-$\mathbf{H_8L}$ ratio of 1:1: (a) **La(H_5L) a**; (b) **La(H_5L) c**; (c) **Nd(H_5L) d** similar to **Gd(H_5L) d**; (d) **Nd(H_5L) b**; (e) **Dy(H_5L) e**.

crystal structure is composed of $[(PO_3H)_2CH-C_6H_4-CH(PO_3H)(PO_3H_2)]^{3-}$ ions, La^{3+} ions, and water molecules. According to the P−O distances (Table S7b), the phosphonate groups around P1, P3, and P4 are singly deprotonated, while the group around P2 is not deprotonated. Additionally, at O1, O5, O6, and O12, hydrogen atoms could be localized and refined. At O7, a hydrogen atom could be found but not be refined. Nd^{3+} is 8-fold-coordinated (Figure 4b, Table S7c). Four coordination sites are occupied by two bisphosphonate groups. The metal ion is chelated via O3 and O4 and via O9 and O10, forming a ring with chair conformation with each bisphosphonate group. Two other phosphonate groups coordinate via O2 and O11, acting as monodentate ligands. The remaining two coordination sites are occupied by the water molecules around O13 and O14. Adjacent Nd^{3+} ions are linked into rows along *a* by bridging phosphonate groups (Figure 4c). The organic linker, which coordinates in bidentate fashion to Nd^{3+} ions of two neighboring rows, extends these chains into a two-dimensional coordination network in the (001) plane (Figure 4d). The phosphonate groups that do not participate in the bridging of the metal polyhedra all stick out to one side of the layer. The layers stack in the *c* direction on top of each other (Figure 4e) and are staggered in the AABB mode. Two adjacent layers are orientated face to face with a short interlayer distance of 5.73 Å. They are joined together by hydrogen bonds between phosphonate groups and the coordinating water molecules of the next layer. Additionally, the free water molecule (O15) assists in the bonding interactions between layers. The distance between such a layer pair is 8.15 Å. Between the layer pairs, the nonbridging phosphonate groups form hydrogen bonds among each other and with the water molecule around O16 (Table S7d).

The second phase whose structure was solved corresponds to **Ln(H_5L) b** (Figure 2). The crystals of **Nd(H_5L) b** are large blocks that grew readily in the concentrated synthesis mixture of the initial high-throughput reaction to an average size of about 100 μm. Under more diluted conditions and at lower temperatures, single crystals of an isotypical compound with La^{3+} as a lattice metal could be obtained (**La(H_5L) b**). The experimental powder pattern of **Nd(H_5L) b** agrees well with the one simulated from the data of the structure solution of **Nd(H_5L) b** and **La(H_5L) b** (Figure S2i). Here, the structure of **La(H_5L) b** will be discussed representatively. With regard to the content of the asymmetric unit, the metal coordination, and the formation of the coordination network, the structure of **La(H_5L) b** coincides with **Ln(H_5L) a**. Only the stacking distance of the layer pairs varies (Figure S6 and Supporting Information, section 6). The nonbridging phosphonate group around P1 is 120° twisted (Figure S6d). This allows the formation of two symmetrical hydrogen bonds, O2−H···O2 and O12−H···O12, and additional hydrogen bridging between the phosphonate group around P1 and the coordinating water molecule around O14 (Table S7g). The distance between the layer pairs decreases from 8.15 to 7.73 Å. The denser packing in the stacking direction may favor the growth of compact blocks over flat needles like in **Nd(H_5L) a**.

Ln(H_5L) a and **Ln(H_5L) b** are very similar. Nevertheless, they have different powder patterns due to their different layer stacking, as do all five phases found in this parameter range. On the other hand, all five phases coincide in the metal-to-ligand ratio, based on EDX analysis. They exhibit similar Raman spectra that confirm the presence of $\mathbf{H_5L}$ in all compounds (Figure 5). **La(H_5L) a** crystallized in the form of fine needles, **La(H_5L) c** as rods, and **Nd(H_5L) b** in the shape of blocks. **Nd(H_5L) d** and **Gd(H_5L) d** both show intergrown platelets, and **Dy(H_5L) e** grows in the shape of small rods (Figure S3a). For all compounds, images at higher magnification revealed features that indicate a layered assembly, such as smooth top faces and lengthwise fissured side faces (Figure 6). Furthermore, thermogravimetric analysis showed that they are very similar in their combustion behavior. They all degrade in three main steps (Figure S5a): After a water loss of about 10%, a second endothermal phase transformation occurs between 300 and 400 °C, until at 600 °C an exothermal oxidative destruction of the carbon network begins. Summarizing all of these features, it can be stated that all five phases show similar two-dimensional coordination frameworks and vary mainly in the stacking mode of their layers. Therefore, they can be combined as isotypical and described with structure type **I** (Figure 2).

Structure Type II. The yellow regions in Figure 1 describe the crystallization fields of layered compounds with the composition **$Ln_2(H_2L)$** which correspond to structure type **II** (Figure 2). Their crystallization was achieved by an increase of the metal-to-ligand ratio. In the La^{3+}-containing system, 4 equiv of NaOH facilitate the crystallization process (Figure 1a). With NaOH, **$La_2(H_2L)$** crystallized between 75 and 100 °C at metal-to-ligand ratios between 2:1 and 6:1. At 150 °C, it could be observed at metal-to-ligand ratios of 4:1 and 6:1. Without NaOH, more drastic conditions were necessary. Then, the formation of **$La_2(H_2L)$** required at 75 °C a metal-to-ligand ratio of 6:1. Between 100 and 150 °C, an excess metal-to-ligand ratio between 4:1 and 6:1 had to be provided. In the Nd^{3+}-containing system, 4 equiv of NaOH are less favorable (Figure 1b). Without NaOH,

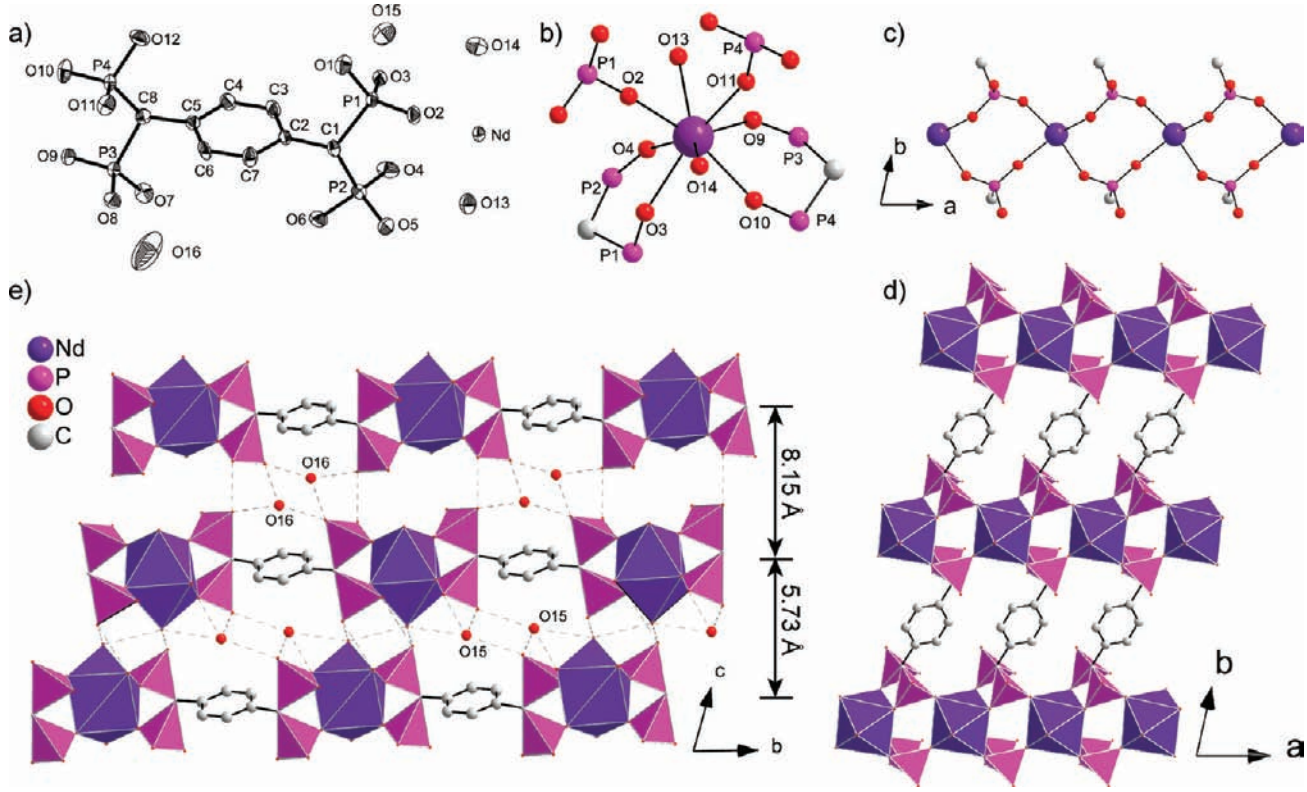

Figure 4. Structure of $Nd[(PO_3H)_2CH-C_6H_4-CH(PO_3H)(PO_3H_2)]\cdot 4H_2O$, **Nd($H_5L$) a** (hydrogens are omitted for clarity): (a) asymmetric unit (thermal ellipsoids are represented with a probability factor of 70%), (b) coordination of Nd^{3+}, (c) phosphonate-bridged chain of Nd^{3+} along *c*, (d) 2D coordination network in the (010) plane, (e) projection along *a* showing a cross section of the layers.

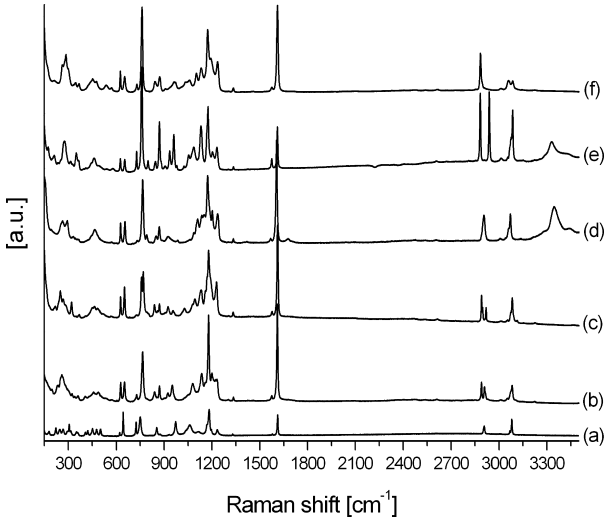

Figure 5. Raman spectra of **H_8L** and the phases crystallized at a lanthanide-to-**H_8L** ratio of 1:1: (a) **H_8L**, (b) **La(H_5L) a**, (c) **La(H_5L) c**, (d) **Nd(H_5L) d**, (e) **Nd(H_5L) b**, (f) **Dy(H_5L) e**.

$Nd_2(H_2L)$ is formed at 75 °C at metal-to-ligand ratios between 4:1and 6:1. From 100 to 150 °C, it could be obtained at metal-to-ligand ratios between 2:1 and 6:1. In the presence of NaOH, **$Nd_2(H_2L)$** crystallized only at 75 °C at a metal-to-ligand ratio of 2:1 and at 100 °C at a metal-to-ligand ratio of 6:1. In the Gd^{3+}-containing system, 4 equiv of NaOH did not have a significant influence, as **$Gd_2(H_2L)$** crystallized with and without NaOH in nearly the whole temperature range at all excess metal-to-ligand ratios (Figure 1c). Exceptions in the presence of NaOH were the metal-to-ligand ratios of 2:1 and 6:1 at 75 °C and the metal-to-ligand ratio

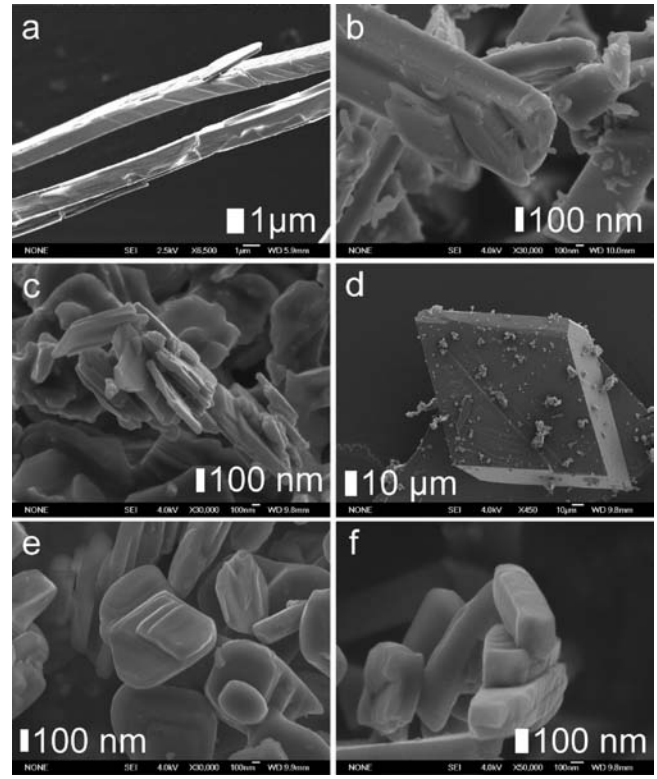

Figure 6. SEM micrographs of compounds crystallized at a batch composition of Ln^{3+}/H_8L = 1:1: (a) **La(H_5L) a**, (b) **La(H_5L) c**, (c) **Nd(H_5L) d**, (d) **Nd(H_5L) b**, (e) **Gd(H_5L) d**, (f) **Dy(H_5L) e** (high magnification).

of 2:1 at 180 °C. Without NaOH, **$Gd_2(H_2L)$** was not formed at the metal-to-ligand ratio of 4:1 at 100 °C nor at the metal

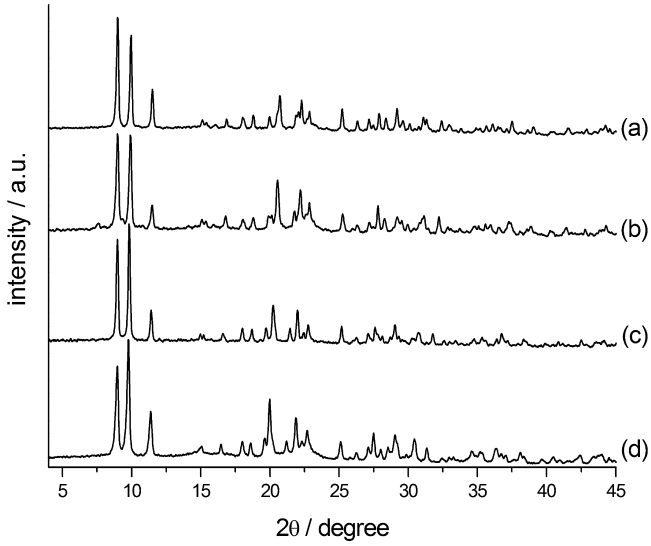

Figure 7. Powder pattern of **$Dy_2(H_2L)$** (a), **$Gd_2(H_2L)$** (b), **$Nd_2(H_2L)$** (c), and **$La_2(H_2L)$** (d).

to ligand ratio of 2:1 at 180 °C. In the Dy^{3+}-containing system, the yellow crystallization field is small compared to those of the other lanthanides (Figure 1d). In the presence of 4 equiv of NaOH, pure-phase **$Dy_2(H_2L)$** was observed at 75 °C at metal-to-ligand ratios between 4:1 and 6:1. At 100 °C, it was formed at a metal-to-ligand ratio of 2:1. Without NaOH, **$Dy_2(H_2L)$** was generated at 100 °C and a metal-to-ligand ratio of 6:1. Furthermore, three unkown phases were observed.

$La_2(H_2L)$, **$Nd_2(H_2L)$**, **$Gd_2(H_2L)$**, and **$Dy_2(H_2L)$** are isomorphous (Figure 7). Raman spectra show that the ligand **H_2L** was incorporated in the structure (Figure S4a). EDX analysis reveals an increased lanthanide-to-ligand ratio of 2:1 (Ln/P = 1:2) for all four compounds. Depending on the reaction media, they crystallize in the shape of large blocks or as intergrown platelets. Single crystalline blocks of **$La_2(H_2L)$** were obtained from concentrated and metal-rich synthesis mixtures (Figure 8a). Under more dilute conditions, **$La_2(H_2L)$** forms agglomerates of twisted sheets (Figure 8b). The structure could be solved from the single crystalline blocks. The simulated theoretical pattern fits well with the experimental data (Figure S2e). Therefore, the structure of **$La_2(H_2L)$** can be discussed exemplarily for structure type **II** (Figure 1).

Single-crystal structure analysis revealed the composition of $La_2[(HO_3P)(O_3P)CH-C_6H_4-CH(PO_3)(PO_3H)]\cdot 8H_2O$. The asymmetric unit contains 17 non-hydrogen atoms and 12 hydrogen atoms. The crystal structure is composed of $[(HO_3P)(O_3P)CH-C_6H_4-CH(PO_3)(PO_3H)]^{6-}$ ions, La^{3+} ions, and water molecules (Figure 9a). According to the P−O distances, the phosphonic acid group around P1 is fully deprotonated and the phosphonic acid group around P2 is only once deprotonated (Table S7h). In good agreement, one hydrogen atom could be located next to O5. The La^{3+} ion has 8-fold coordination geometry (Figure 9b). It is coordinated by two bidentate chelating bisphosphonate units (O2, O1 and O4, O6), one bidentate coordinating phosphonate group (O3, O4), and two water molecules (O7, O8). The phosphonate La−O distances are

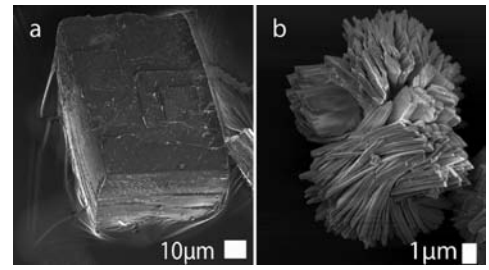

Figure 8. Crystal morphologies of **$La_2(H_2L)$**: (a) single crystalline blocks, (b) twisted sheets.

in the range between 2.66 and 2.44 Å, which is comparable to those reported for $LaPO_4$[50] (Table S7i). The $La-O_{water}$ distances are 2.51 and 2.61 Å. O4 coordinates to two La^{3+} ions. This associates two La^{3+} complexes into dimeric units (Figure 9c). The lanthanum dimers can be represented as two edge-sharing coordination polyhedra; they are connected along (100) into a chain by bridging phosphonate groups (Figure 9d). The chains are linked by the organic spacer of **H_2L**, resulting in a two-dimensional coordination network in the (001) plane. The remaining two crystallographically independent water molecules around O9 and O10 are located between the layers (Figure 9e). The layers stick together by weak interactions such as hydrogen bonds and van der Waals interactions. The interlayer distance is 9.91 Å. In good agreement with this structure description, thermogravimetric analyses of the compounds **$La_2(H_2L)$**, **$Nd_2(H_2L)$**, **$Gd_2(H_2L)$**, and **$Dy_2(H_2L)$** show a weight loss of 16−18% in two endothermic steps between 60 and 150 °C as well as 150 and 250 °C that correspond to the loss of the eight stoichiometric equivalents of water in the structure formula (Figure S5b). The two steps can be explained by the different bonding modes of water. Coordinating water is supposed to leave the structure at higher temperatures compared to free crystal water.

Structure Type III. The red regions in Figure 1 describe the crystallization field of compounds with the composition **$NaLn(H_4L)$** which corresponds to structure type **III** (Figure 2). They crystallize from the batch composition $La^{3+}/H_8L/NaOH = 1:1:4$. Their formation seems strongly favorable and is not affected by either significant temperature changes or a variation of the nature of the lanthanide. This structure type was observed with all four metals and over the whole temperature range. In dilution series, the crystal size of **$NaLa(H_4L)$** could be tuned from 10 to 150 μm. Up to a synthesis temperature of 100 °C, crystals appear nearly square-bipyramidal (Figure 10a). At elevated temperatures of 150 °C, crystal growth becomes faster in one preferential direction. The crystals grew as rods with rhombs on the top and at the bottom (Figure 10b). The crystals of **$NaDy(H_4L)$** showed a curious hole in the middle (Figure 10c). **$NaLa(H_4L)$**, **$NaNd(H_4L)$**, **$NaGd(H_4L)$**, and **$NaDy(H_4L)$** are all isomorphous (Figure 11). Raman spectra show that they incorporate the ligand **H_4L** (Figure S4b). With EDX analysis, in all four

(50) Jaulmes, S. *Bull. Soc. Fr. Mineral. Cristallogr.* **1972**, *95*, 42–6.

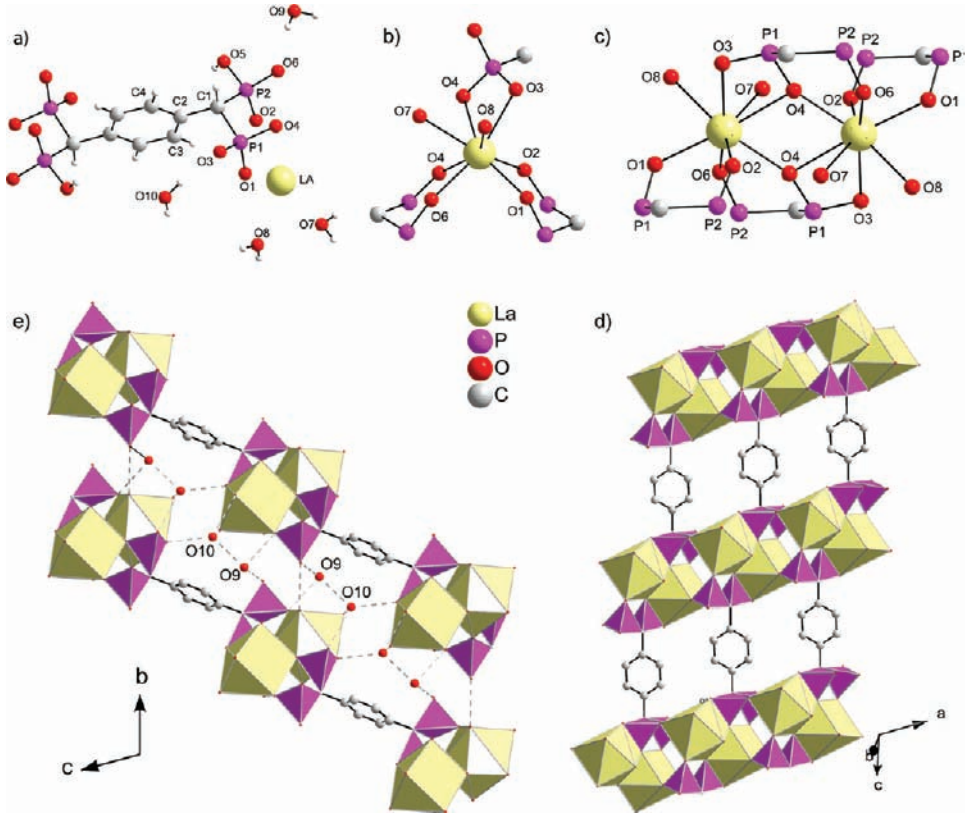

Figure 9. Structure of $La_2[(HO_3P)(O_3P)CH-C_6H_4-CH(PO_3)(PO_3H)]\cdot 8H_2O$, **$La_2(H_2L)$** (hydrogen atoms are omitted for clarity): (a) asymmetric unit with completed molecular fragments, (b) coordination of La^{3+}, (c) association of two La^{3+} ions into a dinuclear cluster via two La−O−La bridges, (d) 2D coordination network, (e) projection along [100] showing a cross section of the layers.

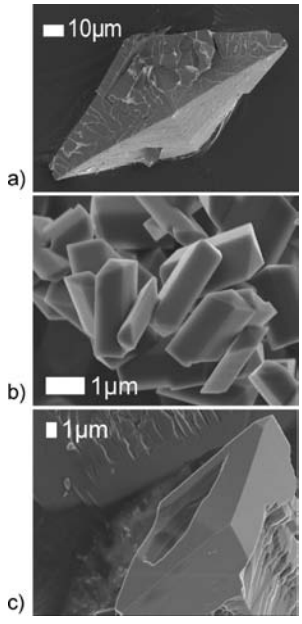

Figure 10. Crystal morphologies of $LnNa[(PO_3H)_2CH-C_6H_4-CH(PO_3H)_2]\cdot 4H_2O$: (a) **$NaLa(H_4L)$** synthesized at 100 °C, (b) **$NaGd(H_4L)$** synthesized at 150 °C, (c) **$NaDy(H_4L)$** synthesized at 150 °C.

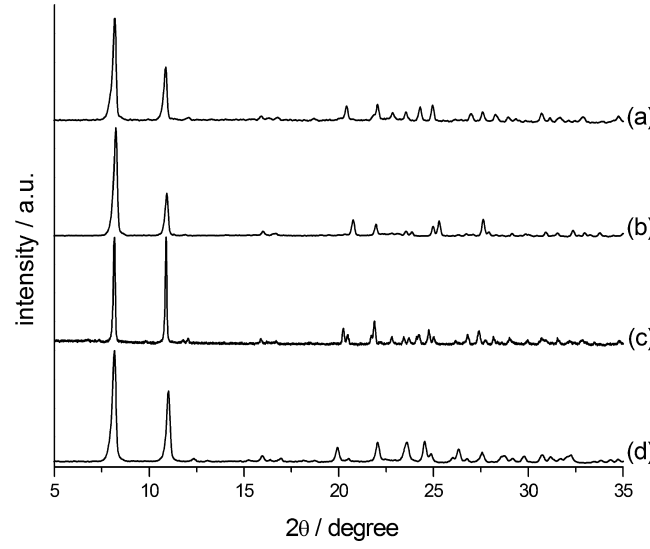

Figure 11. Powder patterns of **$NaDy(H_4L)$** (a), **$NaGd(H_4L)$** (b), **$NaNd(H_4L)$** (c), and **$NaLa(H_4L)$** (d).

compounds, 1 equiv of sodium was detected for each equivalent of lanthanide and ligand.

Single crystals of **$NaLa(H_4L)$** were obtained, and its structure could be resolved. The experimental powder pattern of **$NaLa(H_4L)$** matches very well with the pattern simulated from the structure solution (Figure S2c). Therefore, the structure of **$NaLa(H_4L)$** will be discussed representatively for structure type **III**.

The asymmetric unit of **$NaLa(H_4L)$** contains 29 non-hydrogen atoms and 17 hydrogen atoms (Figure 12a). The crystal structure is composed of $[(PO_3H)_2CH-C_6H_4-CH(PO_3H)_2]^{4-}$ ions, La^{3+} ions, Na^+ ions, and four crystallographically independent water molecules. According to the P−O distances, all four phosphonic acid groups are singly deprotonated (Figure S7k). Additionally, hydrogen atoms

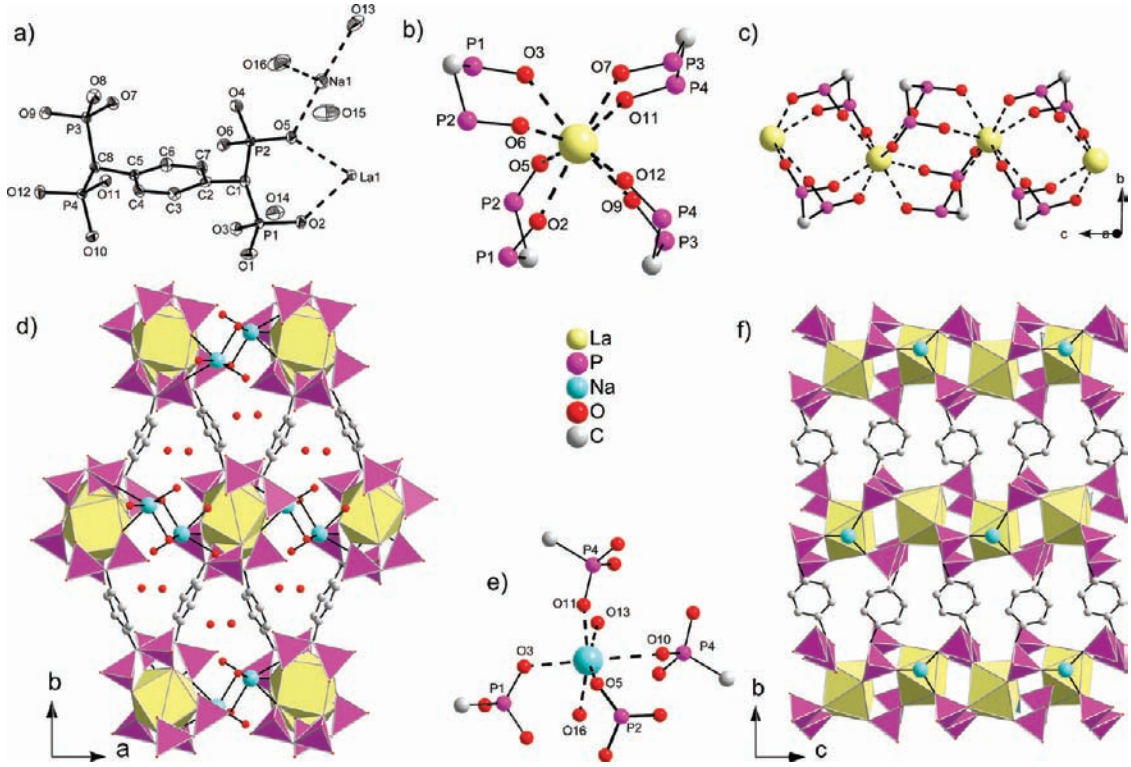

Figure 12. Structure of $LaNa[(PO_3H)_2CH-C_6H_4-CH(PO_3H)_2]\cdot 4H_2O$, **NaLa(H$_4$L)** (hydrogen atoms are omitted for clarity): (a) asymmetric unit (thermal ellipsoids are represented with a probability factor of 70%), (b) coordination of La^{3+}, (c) phosphonate-bridged chain of La^{3+} running along *c*, (d) cross section of the one-dimensional rhombic channels formed by the connection of the chains with the organic spacer, (e) coordination of Na^+, (f) projection along *a* showing the decoration of the chains with sodium ions.

could be refined at O1, O4, O8, and O10. As in structure types **I** and **II**, the La^{3+} ions are 8-fold-coordinated, in this case by phosphonate oxygens from four $(H_4L)^{4-}$ ligands. The La−O distances are between 2.44 and 2.60 Å, which is comparable to those reported for $LaPO_4$[50] (Table S7l). The distinctive feature of structure type **III** is the exclusive coordination of the lanthanide ions by bisphosphonate groups. Four bidentate ligands are chelating one La^{3+} ion, two in the chair and two in the boat conformation (Figure 12b). Additionally, each phosphonate group bridges to a neighboring La^{3+} ion in a way that a chain is built along *c* (Figure 12c). The organic spacer of the ligand connects the chains among each other (Figure 12d and f). The coordinating oxygen atoms around La^{3+} form a square antiprism. The top square of this antiprism is decorated by bisphosphonates around P1 and P2, the bottom square of bisphosphonates around P3 and P4. The coordination geometry of the lanthanide is transferred to the structure of the coordination polymer through the twist angle between the two squares. Thus, a three-dimensional open framework with a one-dimensional channel system along [001] is generated (Figure 12d). Sodium ions and water molecules reside as guests in the channels. Sodium has a strongly distorted octahedral coordination by four phosphonate oxygens and two water molecules (Figure 12e). The Na−O distances range from 2.22 to 2.66 Å (Table S7m).[51] With three bonds, it coordinates to one side of the channel wall. Sodium is connected via O11, O5, and O3 to the triangular side face of the La^{3+} polyhedra alternating on both sides of the chain (Figure 12f). On the side that points into the channel center, Na^+ is coordinated by two water molecules (O13, O16). The sixth interaction with a Na−O distance of 2.67 Å is very weak. It reaches to the chain running on the opposite side of the channel. The two remaining water molecules that do not coordinate to sodium reside as free crystal water above and below the sodium ions in the center of the channels.

Furthermore, compounds with structure type **III** stand out from types **I** and **II** compounds by a distinctive and consistent TGA profile (Figure S5c). Thermogravimetric analysis shows three prominent steps of weight loss for **NaLa(H$_4$L)**, **NaNd(H$_4$L)**, **NaGd(H$_4$L)**, and **NaDy(H$_4$L)**. Step 1 with a weight loss of 11% corresponds to the loss of the four water molecules per asymmetric unit. Remarkably, the temperature necessary for the removal of water increases from La^{3+} (60−160 °C) to Dy^{3+} (110−210 °C). Similar to phases with structure type **I**, an endothermal phase transformation takes place between 300 and 450 °C (step 2). Between 500 and 600 °C, oxidation and combustion of the carbon framework occur in an exothermal third step.

Conclusions

In this study, we could show that **H$_8$L**, providing two bisphosphonate moieties as large chelating ligands that are separated by a phenyl spacer, is a suitable ligand for lanthanides in the synthesis of metal-organic frameworks. In high-throughput screening experiments, we discovered three new structure types of lanthanide tetrakisphosphonates. Structure type **I** is formed by **H$_8$L** with 1 equiv of metal. It

(51) Averbuch-Pouchot, M. T.; Durif, A. *J. Solid State Chem.* **1983**, *46*, 193–6.

comprises various layered structures on the basis of a two-dimensional coordination network where the lanthanide is coordinated by bisphosphonate groups, phosphonate groups, and water molecules. If an excess of lanthanide ions is present during synthesis, compounds with structure type **II** are formed, where the metal centers of the two-dimensional coordination network are associated to dimers. The most interesting structure type emerges when 4 equiv of NaOH are added to the reaction mixture of $\mathbf{H_8L}$, with 1 equiv of metal. With this synthesis stoichiometry, crystals with the three-dimensional open framework of structure type **III** were obtained over a broad range of temperatures and concentrations. In this structure type, a well-defined coordination geometry was achieved with the lanthanide ions coordinated by bisphosphonate units in an exclusively bidentate fashion. This structure features a one-dimensional rhombic channel system with sodium ions and water molecules acting as guests. This shows that the bisphosphonate group connected to an aromatic spacer provides excellent access to MOFs of metals with high coordination numbers that are not easily synthesized with other ligands. $\mathbf{H_8L}$ can be obtained by a general synthesis route that will also permit the preparation of building blocks with larger organic spacers. This would open the way to the synthesis of isoreticular MOFs with the general motif of structure type **III**. Additionally, the expansion of the range of synthesis parameters, which is currently still limited to aqueous media, might lead to new and interesting three-dimensional networks.

Acknowledgment. We thank Peter Mayer from the Department of Chemistry and Biochemistry of the University of Munich for the collection of single-crystal X-ray diffraction data. We thank Steffen Schmidt from the Department of Chemistry and Biochemistry of the University of Munich for extensive SEM and EDX analysis.

Supporting Information Available: Detailed synthesis procedures of each new compound, powder patterns, Raman spectra, SEM micrographs, TGA curves, detailed description of the structure $\mathbf{La(H_5L)b}$, crystallographic details of the structure solutions, selected bond distances, crystallographic data in CIF format. This material is available free of charge via the Internet at http://pubs.acs.org.

IC802294E